

Global Analysis of Solar Neutrinos with Magnetic Moment and Solar Field Profiles

João Pulido *

*Centro de Física das Interações Fundamentais (CFIF)
Departamento de Física, Instituto Superior Técnico
Av. Rovisco Pais, P-1049-001 Lisboa, Portugal*

Abstract

A global statistical analysis of the pre-SNO solar neutrino data including the rates and recoil electron spectrum in SuperKamiokande is made assuming the solar neutrino deficit to be resolved by the interaction of the neutrino magnetic moment with the solar magnetic field. Given the general characteristics of the field profiles known to lead to the best event rate predictions, several specific choices of profiles are assumed and global fits investigated. Whereas previous studies revealed an excellent quality of the rate fits within the magnetic moment solution to the solar neutrino problem, the global fits are found to be only of reasonable quality and comparable to the global oscillation fits. This is related to the difficulty of any theoretical model to provide at present an adjustable prediction to the spectral data.

*E-mail: pulido@beta.ist.utl.pt

Whereas the apparent anticorrelation of the neutrino event rate with sunspot activity claimed long ago by the Homestake collaboration [1] remained unconfirmed by other experiments [2], [3], [4] and theoretical analyses [5], the magnetic moment solution to the solar neutrino problem is at present an important possibility to be explored in the quest for an explanation of the solar neutrino deficit. This is the idea, originally proposed by Cisneros [6], and later revived by Voloshin, Vysotsky and Okun [7], that a large magnetic moment of the neutrino may interact with the magnetic field of the sun, converting weakly active to sterile neutrinos. It now appears in fact that this deficit is energy dependent, in the sense that neutrinos of different energies are suppressed differently. In order to provide an energy dependent deficit, the conversion mechanism from active to nonactive neutrinos must be resonant, with the location of the critical density being determined by the neutrino energy. Thus was developed the idea of the resonant spin flavour precession (RSFP) proposed in 1988 [8]. It involves the simultaneous flip of both chirality and flavour consisting basically in the assumption that the neutrino conversion due to magnetic moment and magnetic field takes place through a resonance inside matter in much the same way as matter oscillations [9]. A sunspot activity related event rate in a particular experiment would hence imply that most of the neutrinos with energies relevant to that experiment have their resonances in the sunspot range. However, the depth of sunspots is unknown (they may not extend deeper than a few hundred kilometers) and the observed field intensity is too small in sunspots to allow for a significant conversion. The anticorrelation argument has therefore lost its appeal for several years now.

Despite the absence of the anticorrelation argument, several main reasons may be invoked to motivate RSFP and investigating its consequences for solar neutrinos. In fact both RSFP and all oscillation scenarios indicate a drop in the survival probability from the low energy (pp) to the intermediate energy neutrino sector (${}^7\text{Be}$, CNO, pep) and a subsequent moderate rise as the energy increases further into the ${}^8\text{B}$ sector. The magnetic field profiles providing good fits to the event rates from solar neutrino experiments typically show the characteristic of a sharp rise in intensity at some point in the solar interior, followed by a progressive moderate decrease [10], [11]. This is in opposite correspondence with the energy dependence of the probability in the sense that the strongest field intensities correspond to the smallest survival probabilities. Hence RSFP offers a unique explanation for the general shape of the probability, which naturally appears as a consequence of the field profile. On the other hand, from solar physics and helioseismology such a sharp rise and peak field intensity is expected to occur along the tachoclyne, the region extending from the upper radiative zone to the lower convective zone, where the gradient of the angular velocity of solar matter is different from zero [12], [13]. Furthermore, it has become clear [14], [10], [11] that RSFP provides event rate fits from the solar neutrino experiments that are far better than all oscillation ones [15], [16]. Finally, there are recent claims in the literature for evidence of a neutrino flux histogram [17] containing two peaks, an indication of variability pointing towards a nonzero magnetic moment of the neutrino.

The aim of this paper is to present a global statistical analysis of three of the field

profiles proposed in [10], all obeying the general features described above, on the light of the updated standard solar model (BP 2000) [18] and the most recent data [1, 2, 3, 4]. This global analysis includes the rates and SuperKamiokande spectrum only, as no day/night variations are expected for RSFP. Since the information on the SuperKamiokande total rate is already present in the flux of each spectral energy bin, this rate will not be included in the analysis, thus following the same attitude as in ref. [19]. The SuperKamiokande energy spectrum used here corresponds to their new data with a range $E_e = (5.0 - 20)MeV$, 19 data points and 1258 days exposure time [2]. Moreover, all Gallium measurements (SAGE, Gallex and GNO) are combined in one single data point. For each profile the local minima of the global χ^2 , defined as $\chi^2_{gl} = \chi^2_{rates} + \chi^2_{spectrum}$, are investigated in the ranges $\Delta m_{21}^2 = (0 - 10^{-7})eV^2$ (mass squared difference between neutrino flavours) and $B_0 = (0 - 300)kG$ (value of the field at the peak). This Δm^2 range is related to neutrino resonances in the region from the upper radiation zone to the solar surface, that is, the whole region where a significant magnetic field is expected. The upper bound of 300 kG for the peak field (B_0) at the base of the convection zone is suggested by most authors [12], [13]. The most poorly known solar neutrino flux, namely hep neutrinos, is taken as a free parameter, whereas the 8B flux is fixed at its BP'2000 value [18]. The χ^2_{gl} local minima occur in the range $\Delta m_{21}^2 = (0.7 - 2.0) \times 10^{-8}eV^2$, with a peak field value from approximately 40kG up and $f_{hep} = \phi(hep)_{(analysis)}/\phi(hep)_{(BP'98)} = 1.07 - 1.46$ where the BP'98 hep flux [20] is taken as the reference one. The values of χ^2_{gl} at these local minima are found to be close to each other and around 20 for 18 d.o.f.. The neutrino magnetic moment is taken at $\mu_\nu = 10^{-11}\mu_B$. This means that, since the order parameter is the product of μ_ν by the magnetic field, for a value of the field at the peak near 300 kG, a suitable magnetic moment solution to the solar neutrino problem may exist at the remarkably low value $\mu_\nu = 1.4 \times 10^{-12}\mu_B$. The results are presented in terms of 2σ (95%CL) and 3σ (99.73%CL) contours on the $\Delta m_{21}^2, B_0$ plane.

The profiles investigated are the following:

Profile (1)

$$B = 0 \quad , \quad x < x_R \quad (1)$$

$$B = B_0 \frac{x - x_R}{x_C - x_R} \quad , \quad x_R \leq x \leq x_C \quad (2)$$

$$B = B_0 \left[1 - \frac{x - x_C}{1 - x_C} \right] \quad , \quad x_C \leq x \leq 1 \quad (3)$$

where x is the fraction of the solar radius and $x_R = 0.70$, $x_C = 0.85$.

Profile (2)

$$B = 0 \quad , \quad x < x_R \quad (4)$$

$$B = B_0 \frac{x - x_R}{x_C - x_R} \quad , \quad x_R \leq x \leq x_C \quad (5)$$

$$B = B_0 \left[1 - \left(\frac{x - 0.7}{0.3} \right)^2 \right] \quad , \quad x_C < x \leq 1 \quad (6)$$

with $x_R = 0.65$, $x_C = 0.75$.

Profile (3)

$$B = 2.16 \times 10^3 \quad , \quad x \leq 0.7105 \quad (7)$$

$$B = B_1 \left[1 - \left(\frac{x - 0.75}{0.04} \right)^2 \right] \quad , \quad 0.7105 < x < 0.7483 \quad (8)$$

$$B = \frac{B_0}{\cosh 30(x - 0.7483)} \quad , \quad 0.7483 \leq x \leq 1 \quad (9)$$

with $B_0 = 0.998B_1$.

The ratios of the RSFP to the SSM event rates $R_{Ga,Ct}^{th}$ are defined as before [10] and the recoil electron spectrum in SuperKamiokande is now

$$R_j^{th} = \frac{\sum_i \int_{E_{ej}}^{E_{ej+1}} dE_e \int_{E'_{em}}^{E'_{eM}} dE'_e f(E'_e, E_e) \int_{E'_m}^{E'_M} dE f_i \phi_i(E) [P(E) \frac{d\sigma_W}{dT'} + (1 - P(E)) \frac{d\sigma_{\bar{W}}}{dT'}]}{\sum_i \int_{E_{ej}}^{E_{ej+1}} dE_e \int_{E'_{em}}^{E'_{eM}} dE'_e f(E'_e, E_e) \int_{E'_m}^{E'_M} dE \phi_i(E) \frac{d\sigma_W}{dT'}} \quad (10)$$

for 19 energy bins ($j=1, \dots, 19$) [2]. Here $\phi_i(E)$ is the SSM neutrino flux for component i ($i = hep, {}^8B$) and the factor f_i is the ratio of the i -th flux relative to the SSM one. For $i = hep$ the reference flux is taken to be the BP'98 one with f_i as a free parameter, while for $i = {}^8B$, for which $\phi_{8B}^{BP'98} = \phi_{8B}^{BP'2000}$, $f_i = 1$ is assumed. The quantity $f(E'_e, E_e)$ is the energy resolution function [21] of the detector in terms of the physical (E'_e) and the measured (E_e) electron energy ($E_e = T + m_e$). The lower limit of E'_e is the detector threshold energy ($E'_{em} = E_{eth}$ with $E_{eth} = 5.0\text{MeV}$) and the upper limit is evaluated from the maximum neutrino energy E_M [10]

$$T'_M = \frac{2E_M^2}{m_e + 2E_M}. \quad (11)$$

For the lower [10] and upper [22] integration limits of the neutrino energy one has respectively

$$E_m = \frac{T' + \sqrt{T'^2 + 2m_e T'}}{2} \quad , \quad E_M = 15\text{MeV} \quad (i = {}^8B) \quad , \quad E_M = 18.8\text{MeV} \quad (i = hep). \quad (12)$$

The weak differential cross sections appearing in equation (17) are given by

$$\frac{d\sigma_W}{dT} = \frac{G_F^2 m_e}{2\pi} [(g_V + g_A)^2 + (g_V - g_A)^2 \left(1 - \frac{T}{E}\right)^2 - (g_V^2 - g_A^2) \frac{m_e T}{E^2}] \quad (13)$$

for $\nu_e e$ scattering, with $g_V = \frac{1}{2} + 2\sin^2\theta_W$, $g_A = \frac{1}{2}$. For $\bar{\nu}_\mu e$ and $\bar{\nu}_\tau e$ scattering,

$$\frac{d\sigma_{\bar{W}}}{dT} = \frac{G_F^2 m_e}{2\pi} [(g_V - g_A)^2 + (g_V + g_A)^2 \left(1 - \frac{T}{E}\right)^2 - (g_V^2 - g_A^2) \frac{m_e T}{E^2}] \quad (14)$$

with $g_V = -\frac{1}{2} + 2\sin^2\theta_W$, $g_A = -\frac{1}{2}$.

The partial event rates for each neutrino component in each experiment were taken from [18] and the solar neutrino spectra from Bahcall's homepage [22]. The contribution of the hep flux to both the Gallium and Homestake event rates was neglected. The χ^2 analysis for the ratios of event rates and electron spectrum in SuperKamiokande was done following the standard procedure described in [10] [†]. The validity of this procedure and alternative ones for solar neutrinos is discussed in refs. [23], [24].

The ratios of event rates to the SSM event rates and the recoil electron spectrum normalized to the SSM one, both denoted by R^{th} in the following, were calculated in the parameter ranges $\Delta m_{21}^2 = (0 - 10^{-7})eV^2$, $B_0 = (0 - 30) \times 10^4 G$ for all magnetic field profiles and inserted in the χ^2 definitions for the rates and spectrum,

$$\chi_{rates}^2 = \sum_{j_1, j_2=1}^2 (R_{j_1}^{th} - R_{j_1}^{exp}) [\sigma_{rates}^2(tot)]_{j_1 j_2}^{-1} (R_{j_2}^{th} - R_{j_2}^{exp}) \quad (15)$$

with (Ga=1, Cl=2)

$$\chi_{sp}^2 = \sum_{j_1, j_2=1}^{19} (R_{j_1}^{th} - R_{j_1}^{exp}) [\sigma_{sp}^2(tot)]_{j_1 j_2}^{-1} (R_{j_2}^{th} - R_{j_2}^{exp}). \quad (16)$$

The quantities R^{exp} in eqs. (15), (16) are directly read from tables I, II respectively and the total error matrices $\sigma^2(tot)$ are derived from the definitions given in [10], using [22] and the error bars in tables I, II. In performing the fitting one has 21 experiments (2 rates and 19 spectral data) and three free parameters, namely the mass squared difference between neutrino flavours Δm_{21}^2 , the peak field value B_0 and the hep flux parametrized by f_{hep} , hence 18 degrees of freedom. With no correlations between the rates and spectral errors one has for the global χ^2 ,

$$\chi_{gl}^2 = \chi_{rates}^2 + \chi_{spectrum}^2. \quad (17)$$

For each of the three profiles, eqs.(1)-(9), the local minima of χ_{gl}^2 in the above parameter ranges were first investigated. Five such minima were found for the equilateral triangle, profile 1, all with $\chi_{gl}^2/18d.o.f. \simeq 20$ (see table III). For the second profile, seven local minima occur with a $\chi_{gl}^2/18d.o.f.$ ranging from 20 to 24 (see table IV) and for the third one only two appear with $\chi_{gl}^2/18d.o.f. = 21 - 22$ (see table V). Each of these minima is obtained for an hep flux from 1.07 to 1.46 of its BP'98 value as also shown. In view of the closeness of the χ^2 values for all these fits with the possible exception of three of them, it is hard to tell which values one should expect the data to prefer. It is clear on the other hand that, since the value of the field at the peak may be as large as 300 kG and this analysis was done using $\mu_\nu = 10^{-11} \mu_B$, a value $B_0 = O(40kG)$ (table III) means the existence of a possible

[†]Here only the main definitions and differences are registered. For the calculational details we refer the reader to ref.[10].

solution to the solar neutrino problem with μ_ν as low as $1.4 \times 10^{-12} \mu_B$ in consistency with astrophysical bounds [25]. Moreover, the fits with the larger B_0 values are disfavoured, as they would imply a value of the neutrino magnetic moment close to $10^{-11} \mu_B$, in conflict with most astrophysical bounds [25].

The allowed physical regions and stability of these fits were also analysed. The results are presented in terms of 2σ and 3σ contours (95% and 99.73% CL respectively) in the $\Delta m_{21}^2, B_0$ plane. These contours enclose the regions for which $\chi^2 \leq \chi_{min}^2 + \Delta\chi^2$ with, for 18 d.o.f., $\Delta\chi^2 = 28.87$ (95%CL) and $\Delta\chi^2 = 39.17$ (99.73%CL) [26]. They are displayed in figs.1, 2, 3 for each of the profiles along with the local χ^2 minima. The dashed lines denote 2σ and the full lines denote 3σ contours. The local minima chosen for reference, that is, the ones for which the contours are defined, are numbers II (profile 1), VI (profile 2) and XIII (profile 3). In view of the closeness of the χ^2 values at the minima, their choice is irrelevant in terms of the difference among contours belonging to different minima: the discrepancies affecting the parameters $\Delta m_{21}^2, B_0$ are hardly perceptible on the scale of the plots. Finally, the contours were worked out for an hep flux (f_{hep}) fixed to its value at the chosen minimum of χ^2 .

As an example, the predicted spectrum (eq.(10)) for profile 3 is shown in fig. 4 at the global best fit (XIII) superimposed on the SuperKamiokande data. For this case $\chi_{sp}^2 = 21.11$. The moderate rise occurring in the theoretical curve for $E_e \geq 12MeV$ is the effect of the hep neutrinos. It is clear from this figure the inherent difficulty in fitting any model prediction to the experimental data, a fact obviously also present in statistical analyses of oscillations.

To conclude, the analysis of prospects for the magnetic moment solution to the solar neutrino problem reveals global fits of reasonable quality. Previous analyses [10], [11],[14] unambiguously indicated from the part of the data on rates a preference for profiles with a steep rise across the bottom of the convection zone in which vicinity they reach a maximum, followed by a more moderate decrease up to the solar surface. This leads to an excellence of rate fits alone which is not shared by the oscillation rate fits. Interestingly enough, this class of profiles is the most consistent one with solar physics and helioseismology [12, 13]. On the other hand the global analysis presented here for rates and spectral data shows a quality of fits comparable to the oscillation ones. This originates from the relative poor quality of the spectrum fits caused by the shape of a function for which no theoretical model is able to provide at present a properly adjustable prediction.

In the present analysis only time averaged data were considered and a fitting was made to a time constant profile 'buried' in the solar interior. If, on the contrary, the active neutrino flux turns out to be time dependent, a situation most likely to be interpreted through the magnetic moment solution with a time dependent interior field, the present approach is obviously inadequate. Averaging the event rates over time implies disregarding possible information in the data which otherwise is available if different periods of time are considered [17]. The robustness of such a procedure will greatly improve with the accumulation of more data.

References

- [1] Homestake Collaboration: B. T. Cleveland *et al.*, *Astrophys. J.* **496**, 505 (1998); B. T. Cleveland *et al.*, *Nucl. Phys. B* (Proc. Suppl.) **38**, 47 (1995); R. Davis, *Prog. Part. Nucl. Phys.* **32**, 13 (1994).
- [2] SuperKamiokande Collaboration: S. Fukuda *et al.*, hep-ex/0103032.
- [3] SAGE Collaboration: V. Gavrin, in *Neutrino 2000*.
- [4] Gallex+GNO Collaboration: E. Bellotti, in *Neutrino 2000*.
- [5] G. Walther, *Phys. Rev. Lett.* **79** 4522 (1998).
- [6] A. Cisneros, *Astrophys. Space Sci.* **10** 87 (1971).
- [7] M. B. Voloshin, M. I. Vysotsky, L. B. Okun, *Soviet J. of Nucl. Phys.* **44** 440 (1986); M. B. Voloshin, M. I. Vysotsky, *Soviet J. of Nucl. Phys.* **44** 544 (1986).
- [8] C. S. Lim and W. J. Marciano, *Phys. Rev.* **D37** 1368 (1988); E. Kh. Akhmedov, *Sov. J. Nucl. Phys.* **48** 382 (1988); E. Kh. Akhmedov, *Phys. Lett.* **B 213** 64 (1988).
- [9] L. Wolfenstein, *Phys. Rev.* **D 17** 2369 (1978); **20** 2634 (1979); S. P. Mikheyev and A. Smirnov, *Sov. J. Nucl. Phys.* **42** 913 (1985).
- [10] J. Pulido, E. Kh. Akhmedov, *Astropart. Phys.* **13** 227 (2000).
- [11] O. G. Miranda, C. Peña Garay, T. I. Rashba, V. B. Semikoz, J. W. F. Valle, *Nucl. Phys.* **B 595** 360 (2001), hep-ph/0005259.
- [12] E. N. Parker in "The Structure of the Sun", *Proc. of the VI Canary Islands School*, Ed. Roca Cortes and F. Sanchez, Cambridge University Press 1996 p. 299.
- [13] H. M. Antia, S. M. Chitre, M. J. Thompson, astro-ph/0005587, to be published in *Astron. and Astrophys.*
- [14] M. Guzzo and H. Nunokawa, *Astropart. Phys.* **12** 87 (1999), hep-ph/9810408.
- [15] J. N. Bahcall, P. I. Krastev and A. Yu. Smirnov, *Phys. Rev.* **D 58** 096016 (1998);
- [16] M.C. Gonzalez-Garcia, P.C. de Holanda, C. Peña-Garay and J.W.F. Valle, *Nucl. Phys.* **B573** 3 (2000), hep-ph/9906469.
- [17] J. Scargle and P. Sturrock, *Ap J* **550** L101 (2001), astro-ph/0011228.
- [18] J. N. Bahcall, M. H. Pinsonneault, S. Basu, astro-ph/0010346, to be published in *Astrophys. Journal*.

- [19] J. N. Bahcall, P. I. Krastev and A. Yu. Smirnov JHEP **0105** 015 (2001), hep-ph/0103179.
- [20] J. N. Bahcall, S. Basu, M. H. Pinsonneault, Phys. Lett. **B433** 1 (1998).
- [21] SuperKamiokande Collaboration, Y. Fukuda *et al.*, Phys. Rev. Lett. **81** 1158 (1998); Erratum-*ibid.* **81** 4279 (1998).
- [22] J. N. Bahcall's homepage, <http://www.sns.ias.edu/~jnb/>.
- [23] M. V. Garzelli and C. Giunti, Proc. of NOW2000, Nucl. Phys. **B** (Proc. Suppl.) **100** (2001) p.77; *ibid.*, hep-ph/0007155.
- [24] P. Creminelli, G. Signorelli and Alessandro Strumia, JHEP **0105** 052 (2001), hep-ph/0102234.
- [25] S. I. Blinnikov, Institute for Theoretical and Experimental Physics Report No. ITEP-88-19 (1988), unpublished; S. I. Blinnikov, V.S. Imshennik, D.K. Nadyozhin, Sov. Sci. Rev. **E** Astrophys. Space Sci. **6**, 185 (1987); G.G. Raffelt, Phys. Rev. Lett. **64** (1990) 2856; Astrophys. J. **365** (1990) 559; V. Castellani and S. Degl'Innocenti, Astrophys. J. **402**, 574 (1993).
- [26] Review of Particle Properties, D. E. Groom *et al.*, The European Physical Journal **C15** 1 (2000).

Experiment	Data	Theory	Data/Theory	Reference
Homestake	$2.56 \pm 0.16 \pm 0.15$	$7.7 \pm_{1.1}^{1.3}$	0.332 ± 0.05	[1]
Ga	74.7 ± 5.13	$129 \pm_6^8$	0.59 ± 0.06	[4],[3]
SuperKamiokande	2.4 ± 0.085	$5.15 \pm_{0.7}^{1.0}$	0.465 ± 0.052	[2]

Table I - Data from the solar neutrino experiments. Units are SNU for Homestake and Gallium and $10^6 cm^{-2} s^{-1}$ for SuperKamiokande. The result for Gallium is the combined one from SAGE and Gallex+GNO.

Energy bin (MeV)	R_i^{exp}
$5 < E_e < 5.5$	0.436 ± 0.046
$5.5 < E_e < 6$	0.438 ± 0.024
$6 < E_e < 6.5$	0.435 ± 0.019
$6.5 < E_e < 7$	0.438 ± 0.015
$7 < E_e < 7.5$	0.463 ± 0.015
$7.5 < E_e < 8$	0.483 ± 0.016
$8 < E_e < 8.5$	0.465 ± 0.017
$8.5 < E_e < 9$	0.438 ± 0.017
$9 < E_e < 9.5$	0.450 ± 0.018
$9.5 < E_e < 10$	0.455 ± 0.019
$10 < E_e < 10.5$	0.442 ± 0.021
$10.5 < E_e < 11$	0.407 ± 0.022
$11 < E_e < 11.5$	0.455 ± 0.026
$11.5 < E_e < 12$	0.423 ± 0.028
$12 < E_e < 12.5$	0.422 ± 0.033
$12.5 < E_e < 13$	0.481 ± 0.041
$13 < E_e < 13.5$	0.431 ± 0.047
$13.5 < E_e < 14$	0.603 ± 0.065
$14 < E_e < 20$	0.493 ± 0.049

Table II - Spectral energy bins in SuperKamiokande (1258 days) and the corresponding ratio of the experimental to the SSM event rate [2].

Fit	$\Delta m_{21}^2 (eV^2)$	$B_0 (G)$	f_{hep}	$\chi_{gl}^2/18d.o.f.$
I	6.68×10^{-9}	4.1×10^4	1.21	21.32
II	6.75×10^{-9}	6.73×10^4	1.19	21.49
III	8.26×10^{-9}	1.34×10^5	1.36	20.22
IV	7.5×10^{-9}	1.7×10^5	1.19	21.37
V	1.0×10^{-8}	2.32×10^5	1.46	19.95

Table III - Local minima of χ_{gl}^2 for profile 1 (eqs.(1)-(3)). The reference for which the 2σ and 3σ contours are determined and drawn in fig.1 is fit II.

Fit	$\Delta m_{21}^2 (eV^2)$	$B_0 (G)$	f_{hep}	$\chi_{gl}^2/18d.o.f.$
VI	1.22×10^{-8}	9.4×10^4	1.24	21.08
VII	1.21×10^{-8}	1.22×10^5	1.07	24.29
VIII	1.28×10^{-8}	1.7×10^5	1.31	20.33
IX	1.3×10^{-8}	1.99×10^5	1.09	23.50
X	1.38×10^{-8}	2.46×10^5	1.43	19.92
XI	1.41×10^{-8}	2.76×10^5	1.11	23.25
XII	1.56×10^{-8}	3.23×10^5	1.45	19.88

Table IV - Local minima of χ_{gl}^2 for profile 2 (eqs.(4)-(6)). The reference for which the 2σ and 3σ contours are determined and drawn in fig.2 is fit VI.

Fit	$\Delta m_{21}^2 (eV^2)$	$B_0 (G)$	f_{hep}	$\chi_{gl}^2/18d.o.f.$
XIII	1.36×10^{-8}	1.04×10^5	1.26	21.24
XIV	1.82×10^{-8}	1.90×10^5	1.17	22.71

Table V - Local minima of χ_{gl}^2 for profile 3 (eqs.(7)-(9)). The reference for which the 2σ and 3σ contours are determined and drawn in fig.3 is fit XIII.

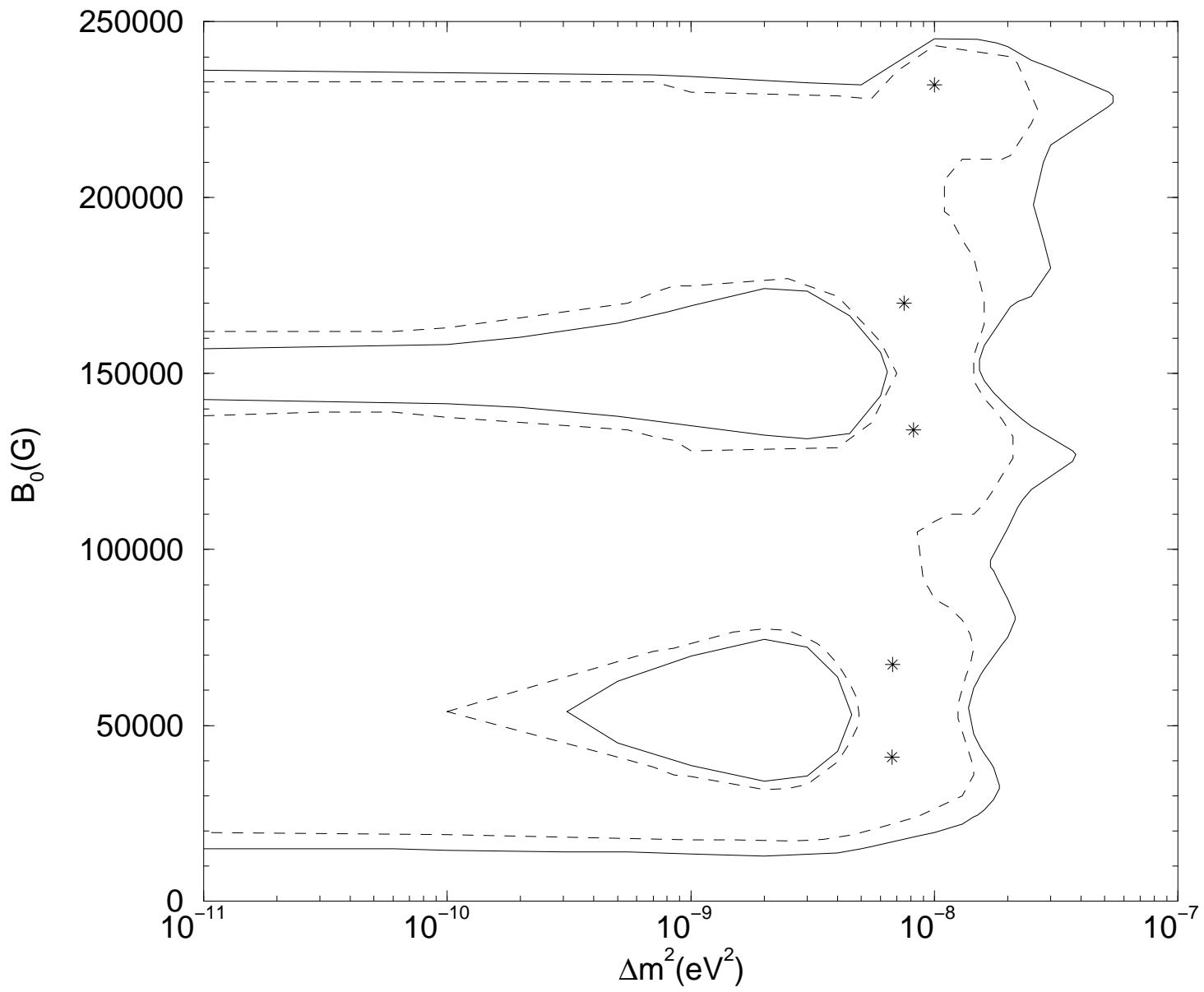
Figure captions

Fig. 1. Fits corresponding to the local minima of χ_{gl}^2 for profile 1 (stars) and the 95% and 99.73%CL contours (dashed and solid lines respectively) with respect to fit II. Since the values of χ_{gl}^2 at these minima lie close to each other (see table III), the contours may be regarded as actually enclosing the common 2σ and 3σ allowed areas on the scale of the plot for all fits.

Fig. 2. Same as fig.1 for profile 2. The reference fit is VI.

Fig. 3. Same as fig.1 for profile 3. The reference fit is XIII.

Fig. 4. The theoretical prediction of the SuperKamiokande recoil electron spectrum (solid line) superimposed on the data set [2] (1258 days) for profile 3 at the global fit XIII. Here the value of χ^2 for the spectrum is $\chi_{sp}^2 = 21.11$.



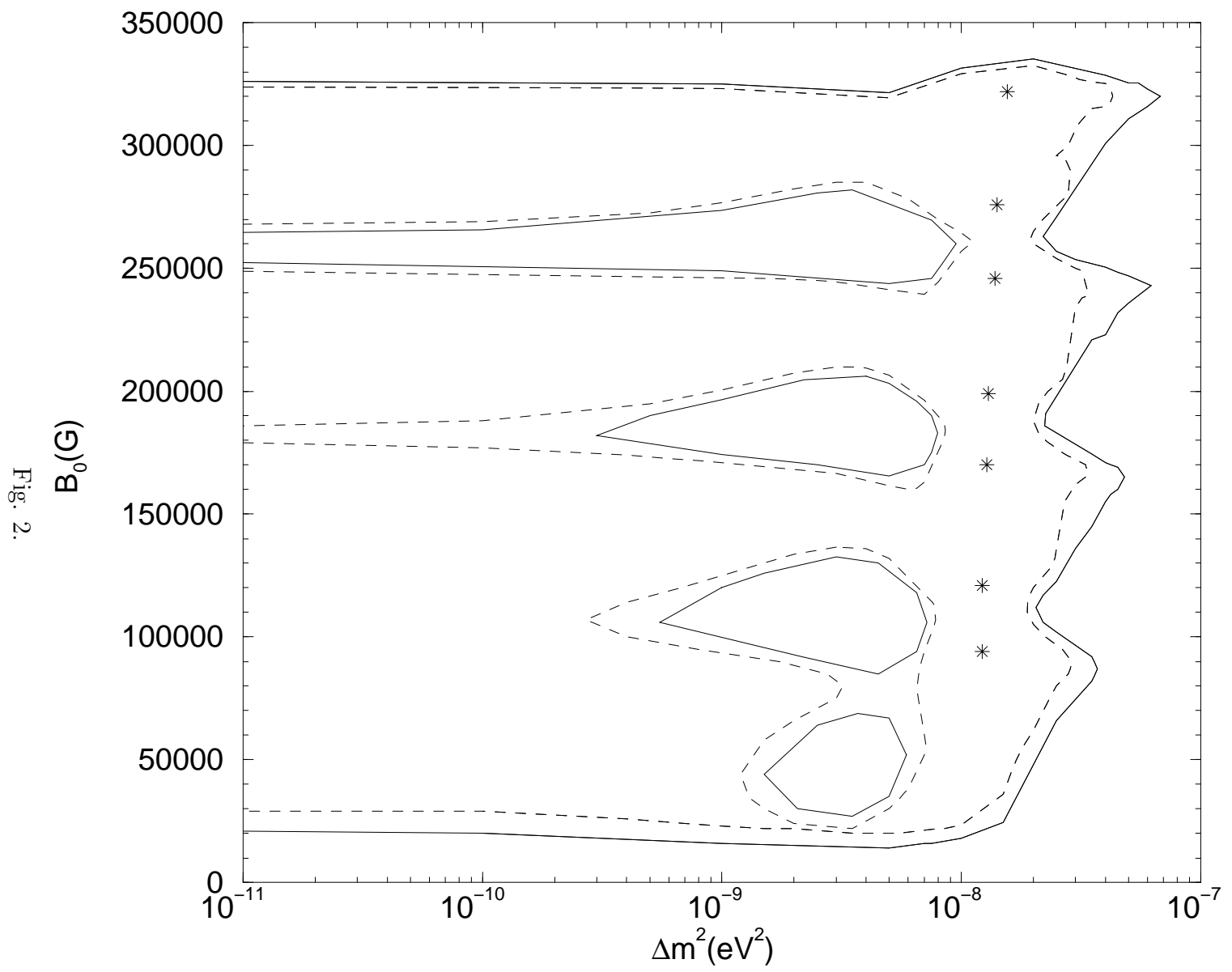
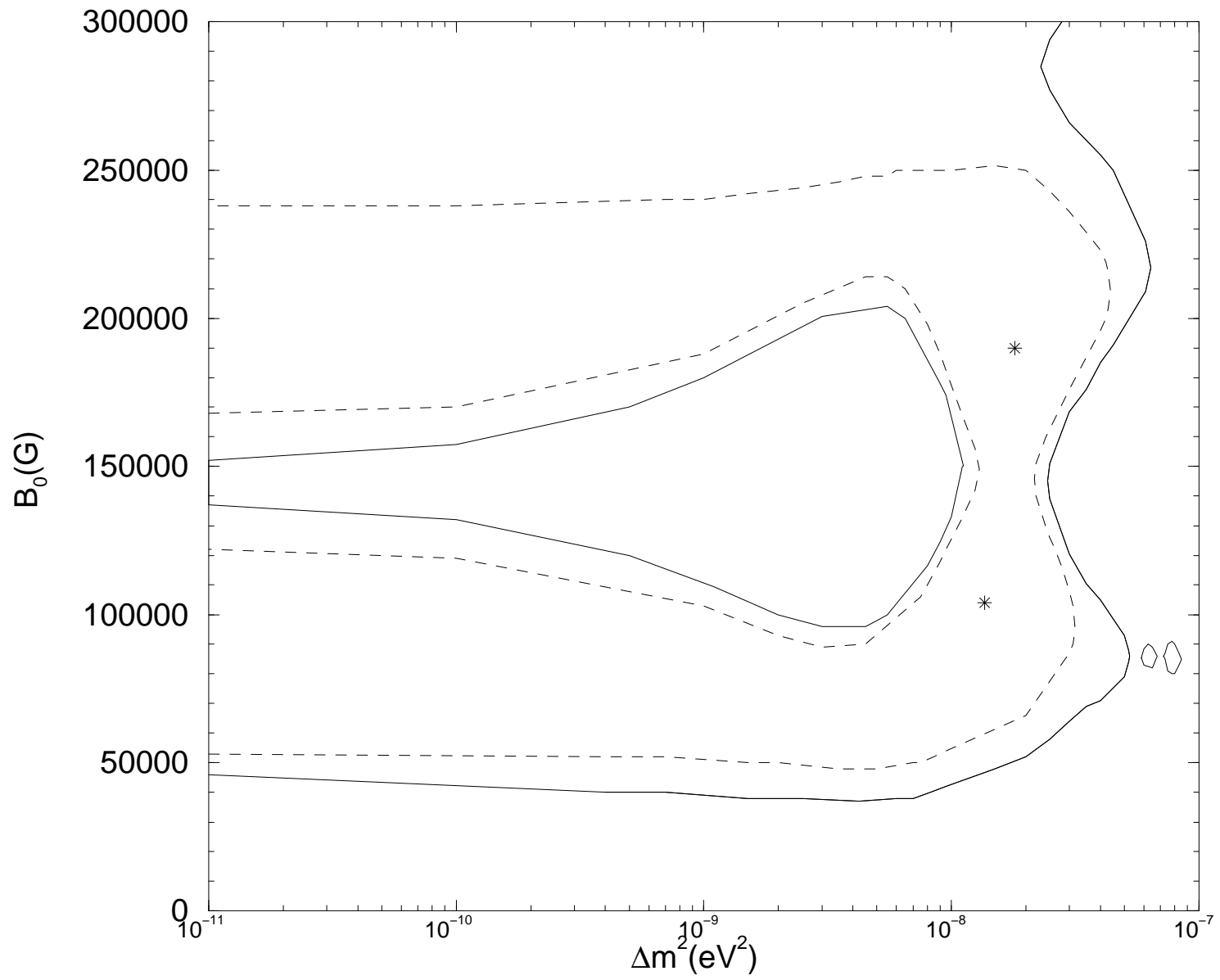


Fig. 2.

Fig. 3.



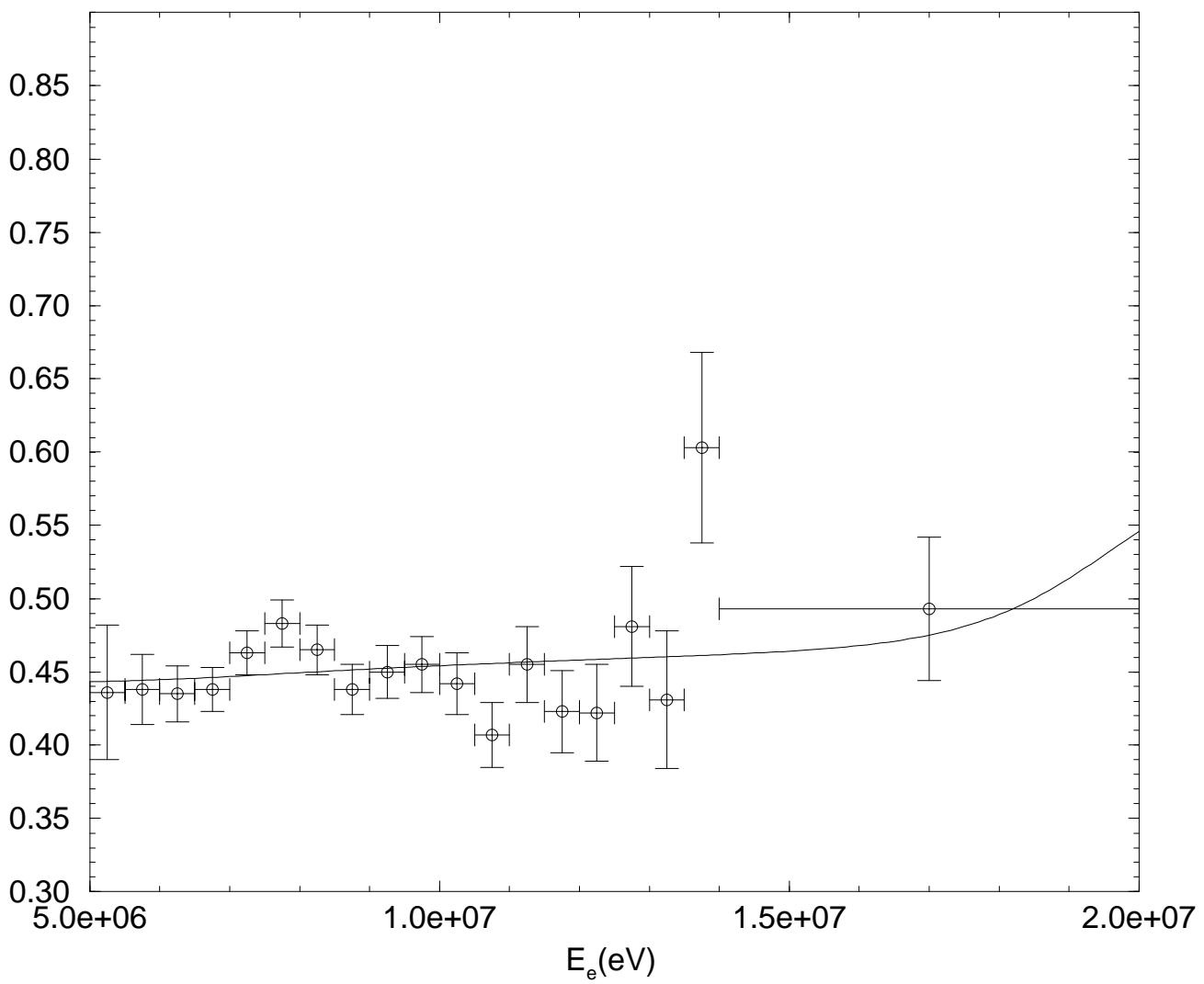


Fig. 4.